electronics

MDPI

Communication

A 0.5 V Nanowatt Biquadratic Low-Pass Filter with Tunable Quality Factor for Electronic Cochlea Applications

Jacek Jakusz and Waldemar Jendernalik *

Faculty of Electronics Telecommunications and Informatics, Gdańsk University of Technology, 80-233 Gdańsk, Poland; jacek.jakusz@pg.edu.pl

* Correspondence: waldemar.jendernalik@pg.edu.pl

Abstract: A novel implementation of an analogue low-power, second-order, low-pass filter with tunable quality factor (Q) is presented and discussed. The filter feature is a relatively simple, buffer-based, circuit network consisting of eleven transistors operating in a subthreshold region. Q tuning is accomplished by injecting direct current into a network node, which changes the output resistance of the transistors and, as a result, modifies the filter network's loss, and thus its Q. Q tuning is independent of a filter cut-off frequency (ω_0). The filter, with a nominal ω_0 of 1 kHz, was fabricated using a 0.18 µm CMOS technology, and features a Q range of 2–11, power consumption of up to 52 nW, and a 59 dB dynamic range when using a 0.5 V supply. The ω_0 can be tuned from 0.5 to 2.5 kHz using a traditional method by changing the transistor transconductances, but this process partially affects the quality factor.

Keywords: analogue filters; low frequency filters; audio filters; low power circuits; analogue integrated circuits; CMOS analogue circuits; electronic cochlea; energy efficient analogue filters

check for updates

Citation: Jakusz, J.; Jendernalik, W. A 0.5 V Nanowatt Biquadratic Low-Pass Filter with Tunable Quality Factor for Electronic Cochlea Applications. *Electronics* **2024**, *13*, 399. https://doi.org/10.3390/electronics13020399

Academic Editors: Nabil Yassine, Abdallah Tammam and Khaled Hayatleh

Received: 21 December 2023
Revised: 15 January 2024
Accepted: 16 January 2024
Published: 18 January 2024

Copyright: © 2024 by the authors. Licensee MDPI, Basel, Switzerland. This article is an open access article distributed under the terms and conditions of the Creative Commons Attribution (CC BY) license (https://creativecommons.org/licenses/by/4.0/).

1. Introduction

One important functional block that is a part of hearing aids [1–6] as well as devices for human voice recognition [7], are tunable filters [8–11] that emulate characteristics of a human cochlea. Such filters allow pre-processing of acoustic signals based on extracting components of the amplitude spectrum of the received sounds and enabling adaptive adjustment of the sensitivity of the signal path in individual frequency bands. Such properties of the filters enable high dynamics and the intelligibility of received sounds, especially human speech, in the presence of noise and external interference, which has a significant impact on the comfort of using a hearing aid and the correctness of human speech recognition. Nowadays, hearing aids are more often manufactured in the form of implants that are placed in the middle ear of hearing-impaired people. In such a case, the problem of reducing power consumption and the voltage supplying the implant becomes particularly important, as the implant itself contains a small store of electrical energy, and its long-term operation relies on the cyclic recharging of energy [6].

Analogue filter implementations (e.g., as in [12–18]) show that analogue filters are more advantageous than fully digital ones from a power reduction perspective. On the other hand, examples of analogue filters realized so far show that it is still difficult to achieve sufficient performance, especially regarding low power consumption, to allow cochlear implant operation without energy charging for many hours. As a result, new, more efficient filter implementations with more favourable parameters are still being researched. Experience from previous implementations of filters in CMOS technology has demonstrated that satisfactory results can be achieved using banks of parallel- [12–14] or cascade- [15–18] connected second-order low-pass filters with electronically tunable quality factor (Q).

Cochlear filter banks typically cover the entire acoustic bandwidth, 20 Hz to 20 kHz, which can be limited to the range of 250 Hz–8 kHz when implementing only the speech

recognition function [19]. Coverage of the required bandwidth is achieved using the appropriate number of filters in a bank, with octave-distributed cut-off frequencies (ω_0). As the volume of the received sound changes, adaptive adjustment of the acoustic sensitivity is realized by means of changes in the quality factor (Q) of individual filters, which is consistent with the physiology of human hearing [20].

The second-order filter presented in this paper was designed for use in cochlear filter banks. Thus, special attention was paid to voltage and power supply reduction and implementation of effective electronic tuning of the quality factor. MOS transistors operating in the subthreshold region with nano ampere bias currents were used to achieve a significant reduction in power consumption. The following sections of this paper describe the filter circuit, the theoretical analysis of the parameters, and measurement results obtained using a prototype filter fabricated using an X-FAB 180-nm CMOS process.

2. Materials and Methods

2.1. Principle of Operation

A detailed schematic of the proposed filter and its transconductance-C model are shown in Figure 1.

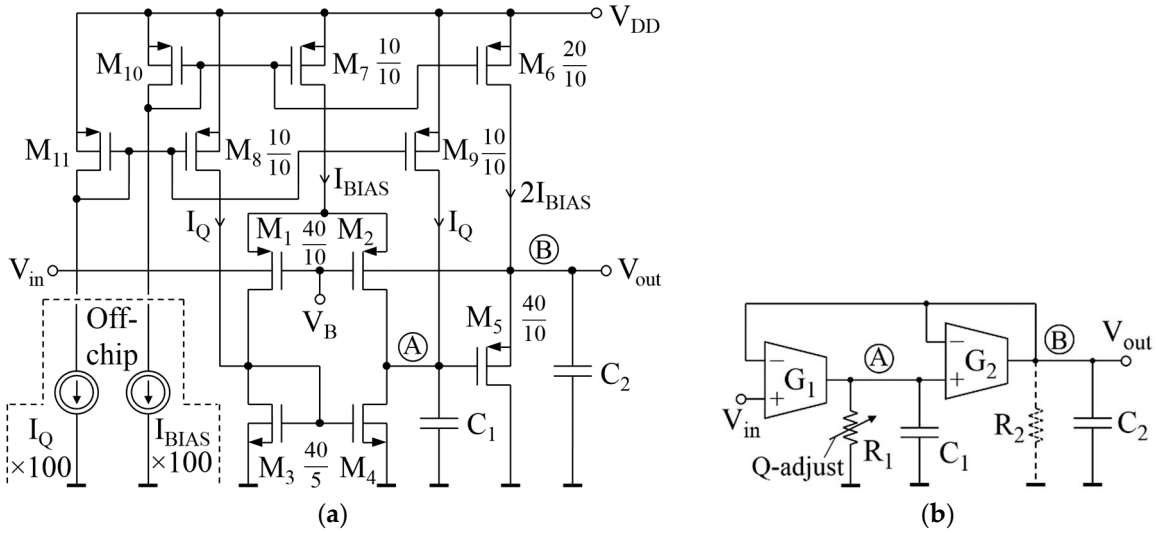

Figure 1. Proposed filter: (**a**) detailed schematic; and (**b**) equivalent small-signal, Gm-C network.

The filter consists of two transconductance stages. The first stage is a differential pair (M_1, M_2) loaded using a current mirror (M_3, M_4) and two extra current sources (M_8, M_9). Due to the low supply voltage (V_{DD}) of 0.5 V, the bulk-driven differential pair is used. The second stage is a source follower (M_5) loaded using a current source (M_6). The stages are modelled using the transconductors G_1 and G_2 in Figure 1b. Their transconductances, G_1 and G_2, are determined by DC bias current I_{BIAS}. The extra DC current I_Q, generated by M_8 and M_9, modifies the resistance seen at node A and, as a result, also modifies the filter quality factor. Nodal resistance is modelled using the adjustable resistor R_1 in Figure 1b.

With I_{BIAS} and I_Q less than 50 nA, all transistors in Figure 1a operate in the subthreshold region. The transistors' gate transconductance (g_m), back-gate transconductance (g_{mbs}), and output conductance (g_{ds}) are proportional to their drain current (I_D) according to the following relationships

$$g_m \cong \frac{I_D}{nV_t},\ g_{mbs} \cong \frac{n-1}{n} g_m = \frac{(n-1)I_D}{n^2 V_t}, g_{ds} \cong I_D \lambda_{DS} \quad (1)$$

where V_t is the thermal voltage, and n and λ_{DS} are technology-dependent parameters [21,22].

MOST WIEDZY Downloaded from mostwiedzy.pl

Thus, the transconductances of the stages are

$$G_1 = g_{mbs1} \cong \frac{(n-1)I_{BIAS}}{2n^2V_t}, G_2 = g_{m5} \cong \frac{I_{BIAS}}{nV_t}, \tag{2}$$

and the nodal resistance is

$$R_1 = \frac{1}{g_{ds4} + g_{ds9} + g_{ds2}} \cong \frac{1}{\lambda_{DS}(I_{D4} + I_{D9} + I_{D2})} = \frac{1}{\lambda_{DS}(I_{BIAS} + 2I_Q)} \tag{3}$$

The resistance at node B, R_2, can be neglected because it is connected in parallel to the resistance $1/G_2$, which is much smaller than R_2; i.e., $1/G_2 << R_2$. With this, the filter transmittance is

$$H(s) = \frac{V_{out}(s)}{V_{in}(s)} = A \cdot \frac{\omega_0^2}{s^2 + s\omega_0/Q + \omega_0^2} \tag{4}$$

where

$$A = 1 - \frac{1}{G_1R_1 + 1}, \ \omega_0 = \sqrt{\frac{(G_1 + 1/R_1)G_2}{C_1C_2}}, \ Q = \frac{\sqrt{(G_1 + 1/R_1)G_2} \cdot \sqrt{\frac{C_1}{C_2}} \cdot R_1}{1 + \frac{C_1}{C_2}G_2R_1} \tag{5}$$

To tune the quality factor effectively, the sensitivity of the Q parameter with respect to R_1 must be greater than the sensitivity of the other filter parameters. This is satisfied if C_2 is much greater than C_1, in details $C_2 >> C_1G_2R_1$ must be met, which is explained in the following section.

2.2. Q Tuning

Thus, assuming that $C_2 >> C_1G_2R_1$, the quality factor Formula (5) becomes

$$Q \overset{C_2>>C_1G_2R_1}{=} \sqrt{(G_1 + 1/R_1)G_2} \cdot \sqrt{\frac{C_1}{C_2}} \cdot R_1 = \omega_0 \cdot C_1 \cdot R_1 \tag{6}$$

The relative sensitivities of the filter parameters with respect to R_1 are

$$S_{R_1}^A = \frac{1}{G_1R_1 + 1}, \ S_{R_1}^{\omega_0} = -\frac{1}{2(G_1R_1 + 1)}, \ S_{R_1}^Q = 1 - \frac{1}{2(G_1R_1 + 1)} \tag{7}$$

where the relative sensitivity is defined as $S_x^y = (dy/y)/(dx/x)$.

As G_1R_1 is much greater than one, $G_1R_1 >> 1$, and the sensitivity of Q to R_1 is several times greater than other sensitivities; i.e., $S_{R_1}^Q >> \left|S_{R_1}^{\omega_0}\right|$ and $S_{R_1}^Q >> S_{R_1}^A$. As a result, the quality factor adjustment only slightly disturbs the cut-off frequency and DC gain.

The condition $C_2 >> C_1G_2R_1$ at (6) is well satisfied in the developed filter, as C_2 is 60 pF, C_1 is 50 fF, and G_2R_1 ranges from 22 to 150.

2.3. ω_0 Tuning

The cut-off frequency ω_0 given by (5) is proportional to I_{BIAS}, $\omega_0 \sim I_{BIAS}$, which results from the facts that conductances G_1, G_2, and $1/R_1$ are $\sim I_{BIAS}$. Using the same facts in (6), it can be deduced that Q should vary moderately when I_{BIAS} changes. The sensitivities of A, ω_0, and Q with respect to I_{BIAS} are as follows

$$S_{I_{BIAS}}^A = \frac{2I_Q}{I_{BIAS}(\eta + 1) + 2I_Q} \cong 0, \quad S_{I_{BIAS}}^{\omega_0} = 1 - \frac{I_Q}{I_{BIAS}(\eta + 1) + 2I_Q} \cong 1, \quad S_{I_{BIAS}}^Q = S_{I_{BIAS}}^{\omega_0} - \frac{I_{BIAS}}{I_{BIAS} + 2I_Q} \tag{8}$$

where $\eta = (n-1)/(2n^2V_t\lambda_{DS})$. When the typical parameters of the process are used (i.e., $n \approx 1.3$, $\lambda_{DS} \approx 0.01$ V^{-1}, and $V_t \approx 25$ mV), the η is about 350. Therefore, the sensitivity of

MOST WIEDZY Downloaded from mostwiedzy.pl

ω_0 to I_{BIAS} is approximately equal to unity and is always greater than the sensitivity of Q to I_{BIAS}.

2.4. Mismatch

Technological mismatch affects all filter components (and hence, filter parameters) according to general rules, and are not analysed in detail here. However, the mismatch related to components C_1 and R_1 requires some comment.

The small capacitor C_1 is exposed to mismatch because of its small area (the Pelgrom rule) and the increased proportion of parasitic capacitances. Fortunately, the sensitivities of the filter parameters with respect to C_1 do not depend on the value of C_1: these sensitivities are constant and less than one; i.e., $S_{C_1}^{\omega_0} = -0.5$, $S_{C_1}^{Q} = 0.5$, and $S_{C_1}^{A} = 0$. Thanks to this, the negative impact of a small C_1 on the filter characteristic is reduced.

As $S_{R_1}^{Q} \cong 1$, deviations in R_1 caused by mismatch directly translate into the spread of the quality factor. The mismatch in R_1 may be relatively high, because R_1 depends on many factors, such as transistor drain currents, channel lengths, λ_{DS} parameter, etc., which are sensitive to mismatch as well. However, detailed Monte Carlo simulations, taking into account all possible mismatch factors, show that ω_0 spreads from 971 to 1023 Hz and Q varies from 21.15 to 21.9 dB, which means that the 1-sigma deviations in ω_0 and Q are 7.95 Hz and 0.12 dB, respectively; i.e., only 0.8% and 0.5%, respectively, with respect to the mean values 0.99 kHz and 21.5 dB, as shown in Figure 2.

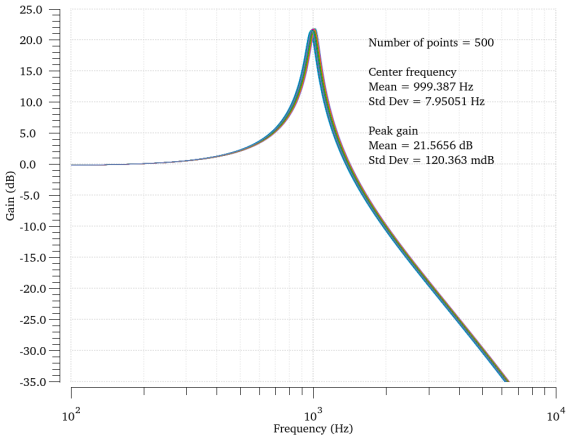

Figure 2. Monte Carlo simulation results (Cadence Spectre) of the 1 kHz filter in Figure 1a.

2.5. Noise

Figure 3a depicts the noise model of the filter. Sources v_{n1} and v_{n2} represent the input-referred noise of the respective amplifiers. The thermal noise of resistor R_1 is assumed to be included in v_{n1} because this resistor is a part of amplifier G_1; i.e., R_1 is the output resistance of this amplifier.

MOST WIEDZY Downloaded from mostwiedzy.pl

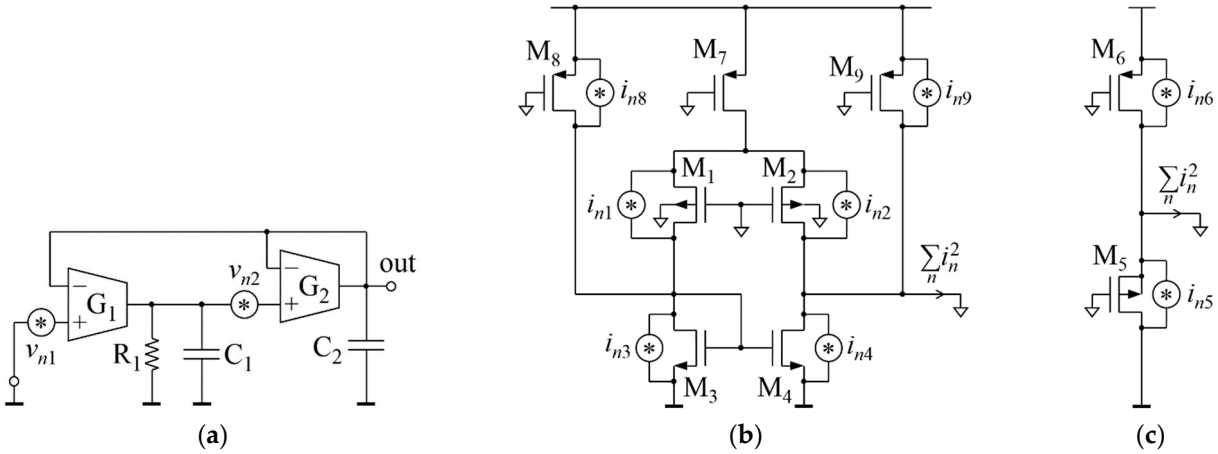

Figure 3. Noise schematics for: (**a**) the whole filter; (**b**) the amplifier G_1; and (**c**) the amplifier G_2.

Based on Figure 3a, the total filter noise (power spectral density) referred to the filter input is

$$v_{n,in}^2(\omega) = \frac{v_{n1}^2(\omega)\cdot|H(j\omega)|^2 + v_{n2}^2(\omega)\cdot|H(j\omega)|^2\cdot\left|\frac{1/R_1+j\omega C_1}{G_1}\right|^2}{|H(j\omega)|^2} = v_{n1}^2(\omega) + v_{n2}^2(\omega)\cdot\frac{\frac{1}{R_1^2}+\omega^2C_1^2}{G_1^2} \quad (9)$$

where $v_{n1}^2(\omega)$ and $v_{n2}^2(\omega)$ denote the power spectral density of the respective noise sources.

Figure 3b,c show the amplifier schematics containing all relevant sources of transistor noise (i_{n7} noise has been neglected, as it is attenuated by a differential stage). Based on these schematics, $v_{n1}^2(\omega)$ and $v_{n2}^2(\omega)$ are

$$v_{n1}^2(\omega) = \frac{\sum i_n^2}{G_1^2} = \frac{i_{n1}^2(\omega)+i_{n2}^2(\omega)+i_{n3}^2(\omega)+i_{n4}^2(\omega)+i_{n8}^2(\omega)+i_{n9}^2(\omega)}{G_1^2},\ v_{n2}^2(\omega) = \frac{\sum i_n^2}{G_2^2} = \frac{i_{n5}^2(\omega)+i_{n6}^2(\omega)}{G_2^2} \quad (10)$$

The Q tuning mechanism introduces extra noise, which is related to the finite resistance R_1 in (9) and the additional noise currents i_{n8} and i_{n9} in (10). The power density of this extra noise can be estimated by calculating the difference in the input-referred noise of the filter with Q tuning, (9), and without one; i.e.,

$$v_{n,in}^2(\omega) - v_{n,in,\textit{without Q tuning}}^2(\omega) = \frac{i_{n8}^2(\omega)+i_{n9}^2(\omega)}{G_1^2} + \frac{i_{n5}^2(\omega)+i_{n6}^2(\omega)}{G_1^2R_1^2G_2^2} \cong \frac{i_{n8}^2(\omega)+i_{n9}^2(\omega)}{G_1^2} \quad (11)$$

Formula (11) shows that the additional noise related to the Q-tuning mechanism is mainly due to the noise generated by transistors M_8 and M_9. As the noise of these transistors increases with their bias current I_Q, a filter variant with low Q has more noise compared to a high-Q variant. The simulated worst-case noise of the 1 kHz (I_{BIAS} = 3 nA) filter in Figure 1a is with a maximal I_Q of 40 nA (Q = 1.9), and is 60 μV_{RMS} when referred to the filter input and integrated from 100 Hz to 1.5 kHz. Assuming no transistors M_8 and M_9, the filter noise is 40 μV_{RMS}, which means that the additional Q-tuning circuit increases the filter noise by 50%.

3. Experiments

3.1. The Chip and Measurements

The filter was implemented in the integrated circuit shown in Figure 4a. A white rectangle indicates an area of the filter, which is 128 µm by 258 µm, including metal-insulator-metal (MIM) capacitors. MIM capacitors cover the entire filter; hence, no transistors are visible in the micro photo.

MOST WIEDZY Downloaded from mostwiedzy.pl

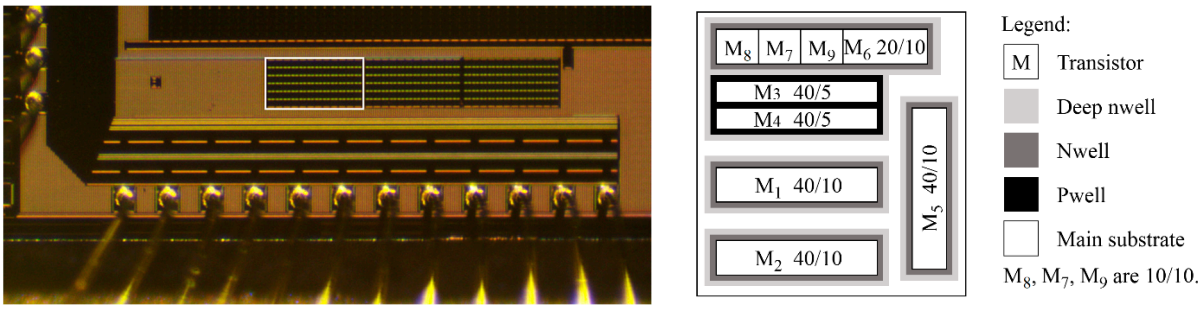

(**a**) (**b**)

Figure 4. Fabricated filter: (**a**) micro photo; and (**b**) simplified view of a filter cell. Transistor dimensions, W/L, are in µm/µm.

The arrangement of transistors inside the filter cell is illustrated in Figure 4b. The filter cell contains transistors M_1 to M_9; their dimensions, W/L in µm/µm, are as follows: M_1 and M_2, 40/10; M_3 and M_4, 40/5; M_5, 40/10; M_6, 20/10; and M_7, M_8, and M_9, 10/10. Transistors M_{10} and M_{11} are outside the cell because they are wide (one hundred parallel-connected 10/10 devices each) to conduct off-chip bias currents. All transistors are thin-oxide low-V_T devices with threshold voltages (V_T) of 0.34 V and −0.39 V for n and p type devices, respectively. Low threshold voltages are necessary due to the 0.5 V supply voltage. As low-V_T transistors have relatively high channel leakage, long 10 µm channels are used, which reduce leakage to much below 0.1 nA at temperatures up to 50 °C.

In the following, measurement results for the filter operating using the supply voltage V_{DD} = 0.5 V, a gate bias voltage V_B = 150 mV, and input DC level of 360 mV are reported.

Figure 5 illustrates the Q tuning process, along with an I_Q ranging from 40 to 0.1 nA. On successive screens from the analyser, it is seen that Q increases from 6.7 dB (2.16) to 21.4 dB (11.74), and there is no deviation in ω_0 (1 kHz). Thus, this observation addresses (7), and confirms that the sensitivity of Q to R_1 is much greater than that of ω_0 to R_1.

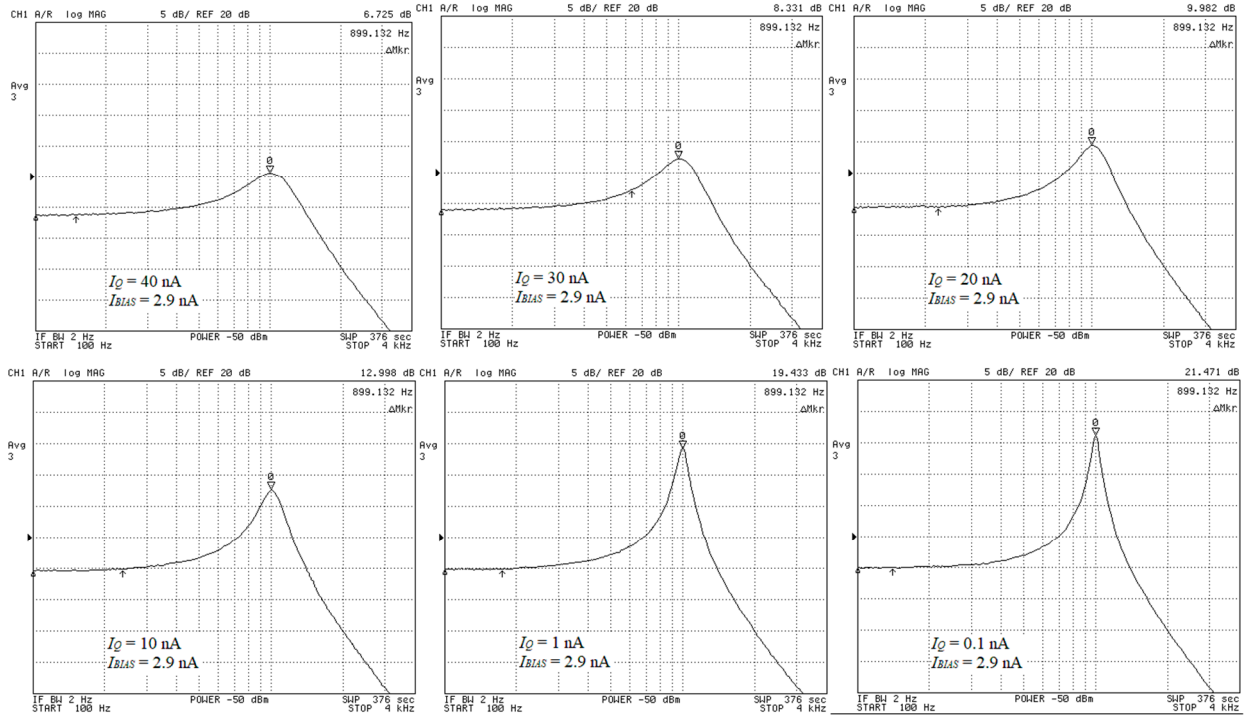

Figure 5. Tuning of Q measured at ω_0 of 1 kHz. I_Q is 40, 30, 20, 10, 1, and 0.1 nA. I_{BIAS} is 2.9 nA.

MOST WIEDZY Downloaded from mostwiedzy.pl

The frequency tuning range was also examined. The consecutive screens in Figure 6 present the measured filter amplitude responses, in which ω_0 increases from 500 Hz to 2.5 kHz, with I_{BIAS} from 1.4 to 7.7 nA. In this case, the quality factor varies due to changes in transistor conductances: the Q deviation is ±12% or ±2%, assuming a tuning range of 0.5–2.5 kHz or 1–1.5 kHz, respectively. Quality factor deviations can be compensated by appropriate corrections of I_Q. For example, ω_0 and Q are 1 kHz and 21 dB, respectively, at an I_{BIAS} of 2.9 nA and an I_Q of 0.1 nA. If ω_0 is set to 1.5 kHz using an I_{BIAS} of 4.5 nA, then I_Q must be corrected to 0.3 nA to maintain the quality factor at the same level.

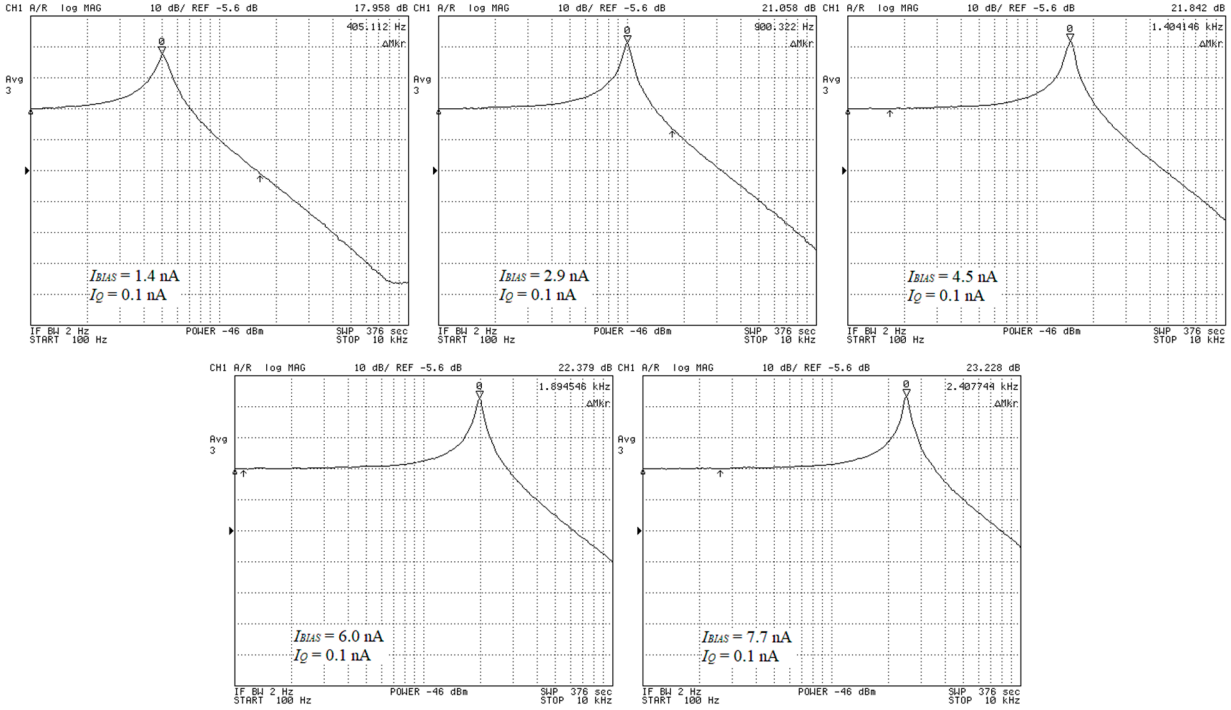

Figure 6. Tuning of ω_0 at Q of 21dB. I_{BIAS} is 1.4, 2.9, 4.5, 6, and 7.7 nA. I_Q is 0.1 nA.

Figure 7a,b show the filter noise density and total-harmonic-distortion (THD) parameter measured at the filter output, respectively. The total noise, referred to the filter input and integrated from 100 Hz to 2 kHz, is 70 μV_{RMS}. The 1% output THD occurs with an input 200 Hz sine wave with an amplitude of 67 mV_{RMS}, which results in a signal-to-noise (S/N) ratio of 59.7 dB.

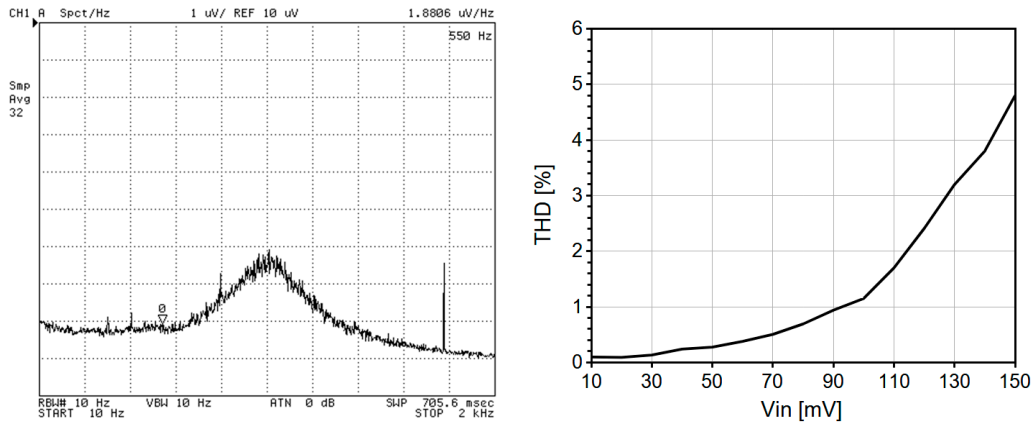

Figure 7. Measured (**a**) output noise of the 1 kHz filter with Q = 2; and (**b**) output THD vs. input amplitude.

Measured filter parameters are summarized in Table 1. Power consumption ranges from 2.2 to 52 nW, depending on the Q and ω_0 values. The power and noise performance of the filter presented in this work are better compared to other solutions, except that of [23]. In terms of quality factor range, the realization of this work meets the minimum requirements for cochlear applications (a Q range of 2–11). The best Q range, 1.3–39, was reported in [14].

Table 1. Performance comparison of low-frequency filters with tunable Q.

Parameter	This Work	[23] Simulated	[18]	[12]	[13]	[14]
Process	0.18 µm	0.18 µm	0.35 µm	0.35 µm	1.5 µm	0.18 µm
Supply	0.5 V	0.5 V	3.3 V	3.3 V	2.8 V	0.5 V
Power	2.2–52 nW	8.25–10.75 nW	NA	13–20 µW [1]	0.1–5.4 µW	0.1–100 nW [2]
ω_0	0.5–2.5 kHz	1.28 kHz	0.1–20 kHz bank	0.31–8 kHz bank	0.2–6 kHz bank	0.08–20 kHz bank
Q	2–11	2–40	NA	2–19	1–10	1.3–39
S/N	59 dB	68 dB	36–52 [3] dB	17–32 dB	57 dB	40–55 dB

[1] Estimated. [2] Estimated assuming no PGA. [3] With PGA.

The frequency tuning range of this work's filter, 0.5–2.5 kHz, cannot be meaningfully compared, because other references report only the frequency range of an entire bank of filters (e.g., 0.1–20 kHz), and not those of individual filters.

The next section discusses the frequency range of a filter bank assuming use of the filter presented in Figure 1a.

3.2. Filter Bank Design Example (Simulations)

A filter bank is a cascade of filters with different nominal cut-off frequencies. To change the nominal cut-off frequency of the filter in Figure 1a, the circuit must be redesigned by appropriately scaling the bias current, capacitance, and transistor dimensions. Taking into account practical design limits, such as a minimum transistor bias current of 0.5 nA (which implies that $I_{BIAS} \geq 1$ nA) and the upper capacitance limit of 100 pF, the cut-off frequency can be scaled down to 500 Hz, according to Table 2.

Table 2. Scaling a filter bank—simulations [1].

ω_0 (kHz)	C_2 (pF)	I_{BIAS} (nA)	M [2]	I_Q (nA)		P (nW)	
				Q = 11.22 (21 dB)	Q = 5.01 (14 dB)	Q = 11.22 (21 dB)	Q = 5.01 (14 dB)
0.5	60	1.42	1	0.025	1.54	2.155	3.67
1	60	2.93	1	0.136	3.1	4.531	7.495
2	30	6.01	2	0.453	6.2	9.468	15.215
4	15	9.12	2	0.198	5.83	13.878	19.51
8	7.5	9.4	2	0.055	5.95	14.155	20.05

[1] Process: X-FAB 180-nm (xh018). Transistors: thin oxide 1.8 V, low VT. [2] Transistor multiplication factor (the number of parallel connected transistors).

On the other side, the upper range of the cut-off frequency is limited by two factors: a minimum value of filter capacitance allowed due to mismatch, and a maximum value of I_{BIAS} related to a power limit. So, based on the worst power case selected from Table 1 (which is [12]), the practical limit of 20 µW per single filter in a bank can be assumed, which is well above the 52 nW achieved in this work. Nevertheless, scaling up I_{BIAS} involves upscaling the transistors' widths (according to scaling factor M in Table 2), which results in a larger parasitic capacitance at node A. This parasite limits the cut-off frequency to 8 kHz, which is quite sufficient for speech recognition systems.

MOST WIEDZY Downloaded from mostwiedzy.pl

4. Discussion

Selecting an appropriate filter structure to build a filter bank is related to the method for tuning the filter quality factor. Depending on the filter structure, the quality factor is adjusted by changing a specific circuit parameter, e.g., the amplifier gain, transconductance, resistance, etc. However, changes in circuit parameters always affect the filter cut-off frequency to a greater or lesser extent. Figure 8 schematically illustrates three different methods of Q tuning: the one proposed in this paper and two others that are applicable to transconductance-C (Gm-C) filter structures. These three methods are briefly discussed and compared.

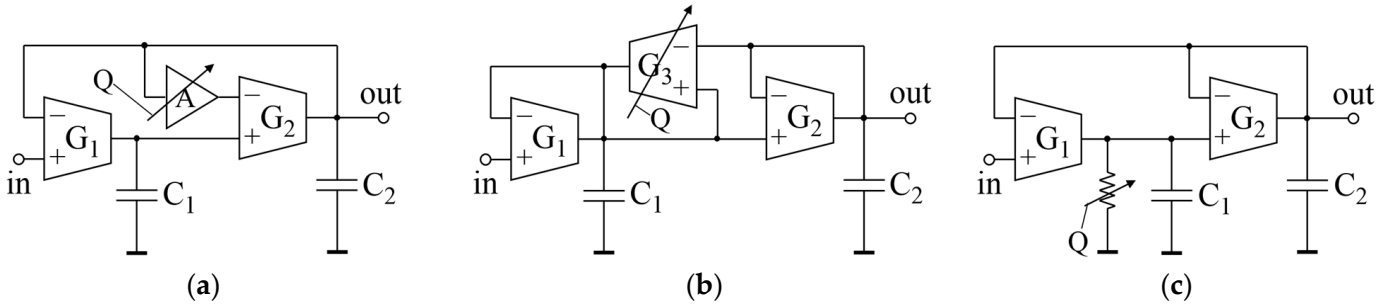

Figure 8. Methods used to tune a quality factor using: (**a**) a voltage attenuator; (**b**) an additional transconductor; and (**c**) a transconductor's output resistance.

The filter shown in Figure 8a uses a loop-in voltage attenuator (A) to tune the quality factor [23]. This method is the only one among those illustrated that allows for fully independent control of the quality factor and cut-off frequency. The disadvantage of this scheme is a certain difficulty in implementing the attenuator, which must attenuate only AC signals, not DC signals.

In the classic method illustrated in Figure 8b, the quality factor is tuned independently by means of the additional transconductance G_3 [16–18,24]. Independent tuning of the cut-off frequency is possible, but G_1/G_2 and G_3/G_2 ratios must be kept constant. Therefore, the robustness of this filter to the transconductance mismatch is weaker compared to that of the other solutions.

The technique proposed in this paper (Figure 8c) uses the adjustable output resistance of a transconductance amplifier to tune the filter quality factor. This is a compromised solution, because the quality factor can be controlled independently, while frequency tuning causes some deviations in the Q factor. The robustness of filter characteristics to technological mismatch is at a satisfactory level despite the capacitance disparity ($C_1 << C_2$), as previously mentioned. The proposed quality factor tuning technique's advantages include relatively simple implementation, because it does not require additional amplifiers, transconductors, etc., but only requires simple DC current sources.

5. Conclusions

The filter presented in this paper can be used to implement low-cost filter banks that emulate the characteristics of the cochlea over the speech frequency range. The proposed filter belongs to the class of buffer-based filters [25] characterized by a DC voltage gain close to unity and an insensitivity to mismatch in the filter passband. Therefore, the proposed filter is suitable for both parallel and cascade banks.

Author Contributions: J.J. and W.J. contributed equally in conceptualization, methodology, formal analysis, simulations, writing—original draft preparation, and writing—review and editing. All authors have read and agreed to the published version of the manuscript.

Funding: This research received no external funding.

Data Availability Statement: Data are contained within the article.

Conflicts of Interest: The authors declare no conflicts of interest.

References

1. Karrenbauer, J.; Klein, S.; Schönewald, S.; Gerlach, L.; Blawat, M.; Benndorf, J.; Blume, H. SmartHeaP—A High-level Programmable, Low Power, and Mixed-Signal Hearing Aid SoC in 22 nm FD-SOI. In Proceedings of the 48th IEEE European Solid State Circuits Conference, ESSCIRC 2022, Milan, Italy, 19–22 September 2022; pp. 265–268. [CrossRef]
2. Raychowdhury, A.; Tokunaga, C.; Beltman, W.; Deisher, M.; Tschanz, J.W.; De, V. A 2.3 nJ/frame voice activity detector-based audio front-end for context-aware system-on-chip applications in 32-nm CMOS. *IEEE J. Solid-State Circuits* **2013**, *48*, 1963–1969. [CrossRef]
3. Price, M.; Glass, J.; Chandrakasan, A.P. A 6 mW, 5000-word real-time speech recognizer using WFST models. *IEEE J. Solid-State Circuits* **2015**, *50*, 102–112. [CrossRef]
4. Yang, G.; Lyon, R.F.; Drakakis, E.M. A 6 µW per channel analog biomimetic cochlear implant processor filterbank architecture with across channels AGC. *IEEE Trans. Biomed. Circuits Syst.* **2015**, *9*, 72–86. [CrossRef] [PubMed]
5. Harczos, T.; Chilian, A.; Husar, P. Making use of auditory models for better mimicking of normal hearing processes with cochlear implants: The SAM coding strategy. *IEEE Trans. Biomed. Circuits Syst.* **2013**, *7*, 414–425. [CrossRef] [PubMed]
6. Yip, M.; Jin, R.; Nakajima, H.H.; Stankovic, K.M.; Chandrakasan, A.P. A Fully-Implantable Cochlear Implant SoC With Piezoelectric Middle-Ear Sensor and Arbitrary Waveform Neural Stimulation. *IEEE J. Solid-State Circuits* **2015**, *50*, 214–229. [CrossRef] [PubMed]
7. Russo, M.; Stella, M.; Sikora, M.; Pekić, V. Robust Cochlear-Model-Based Speech Recognition. *Computers* **2019**, *8*, 5. [CrossRef]
8. Ma, T.; Shen, C.; Wei, Y. Adjustable Filter Bank Design for Hearing Aids System. In Proceedings of the 2019 IEEE International Symposium on Circuits and Systems, ISCAS 2019, Sapporo, Japan, 26–29 May 2019; pp. 1–5. [CrossRef]
9. Wei, Y.; Ma, T.; Ho, B.K.; Lian, Y. The Design of Low-Power 16-Band Nonuniform Filter Bank for Hearing Aids. *IEEE Trans. Biomed. Circuits Syst.* **2019**, *13*, 112–123. [CrossRef] [PubMed]
10. Özbek, B.; Külah, H. A 1-V Nanopower Highly Tunable Biquadratic $G_m - C$ Bandpass Filter for Fully Implantable Cochlear Implants. In Proceedings of the 2021 IEEE Biomedical Circuits and Systems Conference, BioCAS 2021, Berlin, Germany, 6–9 October 2021; pp. 1–5. [CrossRef]
11. Özbek, B.; Külah, H. A 9.03 µW Low Noise Highly Tunable Analog Front-End for Fully Implantable Cochlear Prosthesis. In Proceedings of the 2022 IEEE Biomedical Circuits and Systems Conference, BioCAS 2022, Taipei, Taiwan, 13–15 October 2022; pp. 349–353. [CrossRef]
12. Wang, S.; Koickal, T.J.; Hamilton, A.; Cheung, R.; Smith, L.S. A bio-realistic analog CMOS cochlea filter with high tunability and ultra-steep roll-off. *IEEE Trans. Biomed. Circuits Syst.* **2015**, *9*, 297–311. [CrossRef] [PubMed]
13. Sarpeshkar, R.; Salthouse, C.; Sit, J.J.; Baker, M.W.; Zhak, S.M.; Lu, T.T.; Turicchia, L.; Balster, S. An ultra-low-power programmable analog bionic ear processor. *IEEE Trans. Biomed. Eng.* **2005**, *52*, 711–727. [CrossRef] [PubMed]
14. Yang, M.; Chien, C.-H.; Delbruck, T.; Liu, S.-C. A 0.5 V 55 µW 64 × 2 Channel Binaural Silicon Cochlea for Event-Driven Stereo-Audio Sensing. *IEEE J. Solid-State Circuits* **2016**, *51*, 2554–2569. [CrossRef]
15. Lyon, R.F.; Mead, C. An analog electronic cochlea. *IEEE Trans. Acoust. Speech Signal Process* **1988**, *36*, 1119–1134. [CrossRef]
16. Watts, L.; Kerns, D.A.; Lyon, R.F.; Mead, C.A. Improved implementation of the silicon cochlea. *IEEE J. Solid-State Circuits* **1992**, *27*, 692–700. [CrossRef]
17. Sarpeshkar, R.; Lyon, R.F.; Mead, C.A. An analog VLSI cochlea with new transconductance amplifiers and nonlinear gain control. In Proceedings of the 1996 IEEE International Symposium on Circuits and Systems, Circuits and Systems Connecting the World, ISCAS 96, Atlanta, GA, USA, 15 May 1996; Volume 3, pp. 292–296. [CrossRef]
18. Liu, S.-C.; van Schaik, A.; Minch, B.A.; Delbruck, T. Asynchronous binaural spatial audition sensor with 2 × 64 × 4 channel output. *IEEE Trans. Biomed. Circuits Syst.* **2014**, *8*, 453–464. [CrossRef] [PubMed]
19. Suzuki, Y.; Takeshima, H. Equal-loudness-level contours for pure tones. *J. Acoust. Soc. Am.* **2004**, *116*, 918–933. [PubMed]
20. Ruggero, M.A.; Shyamla Narayan, S.; Temchin, A.N.; Recio, A. Mechanical bases of frequency tuning and neural excitation at the base of the cochlea: Comparison of basilar-membrane vibrations and auditory-nerve-fiber responses in chinchilla. *Proc. Natl. Acad. Sci. USA* **2000**, *97*, 11744–11750. [CrossRef] [PubMed]
21. Alioto, M. Ultra-Low Power VLSI Circuit Design Demystified and Explained: A Tutorial. *IEEE Tran. Circuits Syst. II Reg. Pap.* **2012**, *59*, 3–29. [CrossRef]
22. Enz, C.; Krummenacher, F.; Vittoz, E.A. An analytical MOS transistor model valid in all regions of operation and dedicated to low-voltage and low-current applications. *J. Anal. Integr. Circuits Signal Process* **1995**, *8*, 83–114. [CrossRef]
23. Jendernalik, W.; Jakusz, J.; Blakiewicz, G. Low-Voltage Low-Power Filters with Independent ω_0 and Q Tuning for Electronic Cochlea Applications. *Electronics* **2022**, *11*, 534. [CrossRef]

MOST WIEDZY Downloaded from mostwiedzy.pl

24. Grech, I.; Micallef, J.; Azzopardi, G.; Debono, C.J. A 0.9 V wide-input-range bulk-input CMOS OTA for GM-C filters. In Proceedings of the 10th IEEE International Conference on Electronics, Circuits and Systems, ICECS 2003, Sharjah, United Arab Emirates, 14–17 December 2003; Volume 2, pp. 818–821. [CrossRef]
25. Jendernalik, W.; Jakusz, J.; Blakiewicz, G. Ladder-Based Synthesis and Design of Low-Frequency Buffer-Based CMOS Filters. *Electronics* **2021**, *10*, 2931. [CrossRef]

Disclaimer/Publisher's Note: The statements, opinions and data contained in all publications are solely those of the individual author(s) and contributor(s) and not of MDPI and/or the editor(s). MDPI and/or the editor(s) disclaim responsibility for any injury to people or property resulting from any ideas, methods, instructions or products referred to in the content.

MOST WIEDZY Downloaded from mostwiedzy.pl